

A split spectrum processing of noise-contaminated wave signals for damage identification

X.T. Miao¹, Lin Ye², F.C. Li^{*1}, X.W. Sun¹, H.K. Peng³, Ye Lu² and Guang Meng¹

¹State Key Laboratory of Mechanical System and Vibration, Shanghai Jiao Tong University, Shanghai 200240, China

²Laboratory of Smart Materials and Structures (LSMS), Centre for Advanced Materials Technology (CAMT), School of Aerospace, Mechanical and Mechatronics Engineering, The University of Sydney, NSW 2006, Australia

³Shanghai Institute of Satellite Engineering, Shanghai 200240, China

(Received May 25, 2011, Revised June 25, 2012, Accepted July, 22, 2012)

Abstract. A split spectrum processing (SSP) method is proposed to accurately determine the time-of-flight (ToF) of damage-scattered waves by comparing the instantaneous amplitude variation degree (IAVD) of a wave signal captured from a damage case with that from the benchmark. The fundamental symmetrical (S_0) mode in aluminum plates without and with a notch is assessed. The efficiency of the proposed SSP method and Hilbert transform in determining the ToF of damage-scattered S_0 mode is evaluated for damage identification when the wave signals are severely contaminated by noise. Broadband noise can overwhelm damage-scattered wave signals in the time domain, and the Hilbert transform is only competent for determining the ToF of damage-scattered S_0 mode in a noise-free condition. However, the calibrated IAVD of the captured wave signal is minimally affected by noise, and the proposed SSP method is capable of determining the ToF of damage-scattered S_0 mode accurately even though the captured wave signal is severely contaminated by broadband noise, leading to the successful identification of damage (within an error on the order of the damage size) using a triangulation algorithm.

Keywords: split spectrum processing (SSP); instantaneous amplitude variation degree (IAVD); time of flight (ToF); guided waves; broadband noise; triangulation algorithm

1. Introduction

Guided wave such as Lamb waves has shown great effectiveness in the field of nondestructive evaluation (NDE) over the past two decades (Wang *et al.* 2007, Lu *et al.* 2010). However, because environmental noise severely decreases the signal-to-noise ratio (SNR), it can be very difficult to determine genuine time of flight (ToF) of damage-scattered waves from raw captured wave signals. Signal processing techniques play a critical role in guided wave-based damage identification, significantly influencing the precision and applicability of any inverse algorithm that requires precise determination of the ToF, such as the triangulation algorithm (Su *et al.* 2007, Su *et al.* 2009). Various signal processing techniques have been developed to enhance SNR, exemplified by

*Corresponding author, Ph.D., E-mail: fccli@sjtu.edu.cn

Hilbert-Huang transform (HHT) (Quek *et al.* 2003) and wavelet transform (WT) (Ip *et al.* 2004, Pardo *et al.* 2006, Li *et al.* 2009). After being properly de-noised, damage-scattered waves can be interpreted by referring to the benchmark wave signal. The ToF of damage-scattered waves can thus be determined based on their energy peak by using the Hilbert transform (Michaels 2008, Lu *et al.* 2010). However, unexpected noise energy cannot be excluded effectively using such signal processing techniques when the noise is broadband and located in the main frequency band of the captured wave signals, increasing the difficulty of determining the ToF.

The split spectrum processing (SSP) method was initially introduced to determine the ToF of target echo during ultrasonic wave-based NDE (Ericsson *et al.* 1992), based on the fact that when the target echo appears in the captured signal, coherent amplitude will be present among a series of time scale signals which are constructed for the captured signal using IFFT (Bosch *et al.* 2005, Benammar *et al.* 2008). During SSP, the amplitude coherence among the series of time scale signals is assessed at each sampling time point, then the moment with good amplitude coherence correspond to the appearance of the target echo and its ToF is determined using appropriate feature extraction algorithm. It has been proved that the amplitude coherency is nearly not influenced by noise and therefore SSP can ensure effective determination of the ToF for the target echo in a captured signal even when there is a low SNR (Ericsson *et al.* 1992).

In this study, the SSP method was proposed to determine the ToF of damage-scattered waves, in particular when the captured wave signal was overwhelmed by indeterminate noise. During SSP, the instantaneous amplitude variation range among the series of constructed time scale signals was defined as the instantaneous amplitude variation degree (IAVD) of the captured wave signal. A feature extraction algorithm was developed to define the ToF of the S_0 mode scattered by a notch in an aluminum plate by comparing the IAVD of the captured wave signal for the damage case with that for the benchmark. With the ToF determined from individual sensing paths of an active sensor network, the notch was successfully identified using a triangulation algorithm.

2. Principles and fundamentals

2.1 ToF-based triangulation algorithm

Lamb waves, a kind of guided waves propagating in plate-like structures, consist of two groups of modes (symmetrical and anti-symmetrical), and each propagates at its own velocity. The S_0 mode is normally used in various studies because it has the highest propagation velocity at frequency range lower than 500 kHz for the discussed plate of 2 mm thickness, avoiding the disturbance of other modes (Giurgiutiu 2005, Wang *et al.* 2007, Lu *et al.* 2010). ToF is one of the straightforward features of a guided wave signal for damage identification. With ToFs of damage-scattered waves determined from a certain number of sensing paths of an active sensor network, the damage location can be defined using a triangulation algorithm (Kessler *et al.* 2002, Su *et al.* 2002, Diamanti *et al.* 2005). For an S_0 mode activated by an actuator and captured by a sensor, as shown in Fig. 1(a), when the propagation group velocity is same for the incident and damage-scattered S_0 mode (provided that no mode conversion occurs) the ToF of the damage-scattered S_0 mode can be described as:

$$T_D = T_{A-D-S} - T_{A-S} = (L_{A-D} + L_{D-S} - L_{A-S}) / v_g \quad (1)$$

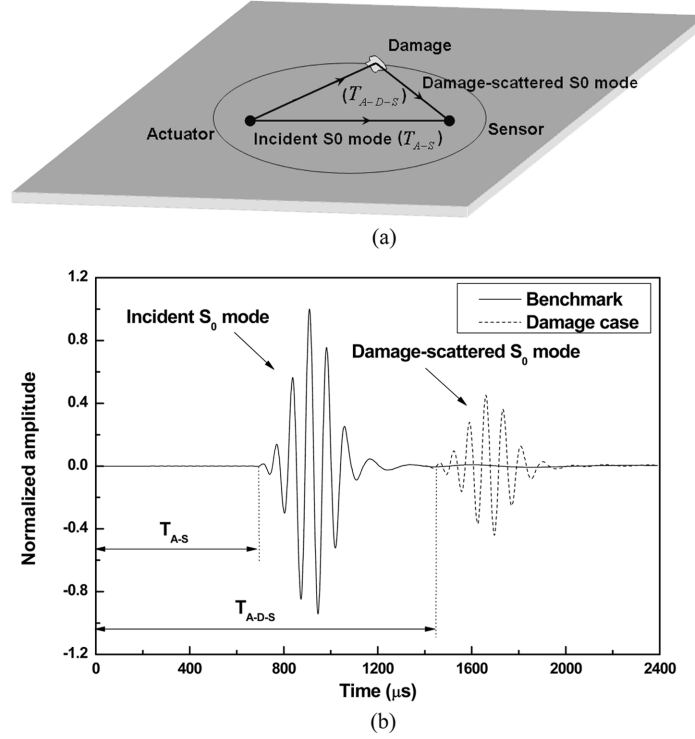


Fig. 1 Schematic diagram of (a) the triangulation algorithm and (b) T_{A-S} and T_{A-D-S}

where

$$\begin{aligned}
 L_{A-D} &= \sqrt{(x_A - x_D)^2 + (y_A - y_D)^2} \\
 L_{D-S} &= \sqrt{(x_D - x_S)^2 + (y_D - y_S)^2} \\
 L_{A-S} &= \sqrt{(x_A - x_S)^2 + (y_A - y_S)^2}
 \end{aligned}
 \tag{2}$$

T_{A-D-S} is the ToF of the incident S_0 mode propagating from an actuator to the damage and then to a sensor; and T_{A-S} is the ToF of the incident S_0 mode propagating directly from the actuator to the sensor, as shown in Fig. 1 Schematic diagram of (a) the triangulation algorithm and (b) and (b). L_{A-D} is the distance between the actuator located at (x_A, y_A) and the damage center which is presumed at (x_D, y_D) and to be identified; L_{D-S} is the distance between the damage center and the sensor located at (x_S, y_S) ; and L_{A-S} is the distance between the actuator and the sensor. v_g is the propagation group velocity of the incident and damage-scattered S_0 mode. The solutions to Eq. (1) configure a locus that is an ellipse with the actuator and sensor as its two foci, indicating the possible location of the damage edge which scatters the incident S_0 mode first (Su *et al.* 2009). The location(s) with the most intersections of multiple loci configured by multiple sensing paths of an active sensor network is(are) where the damage is most likely to be present.

2.2 Split-spectrum processing (SSP)

Generally speaking, a captured signal, $r(t)$, includes the target echoes (i.e., the incident wave when

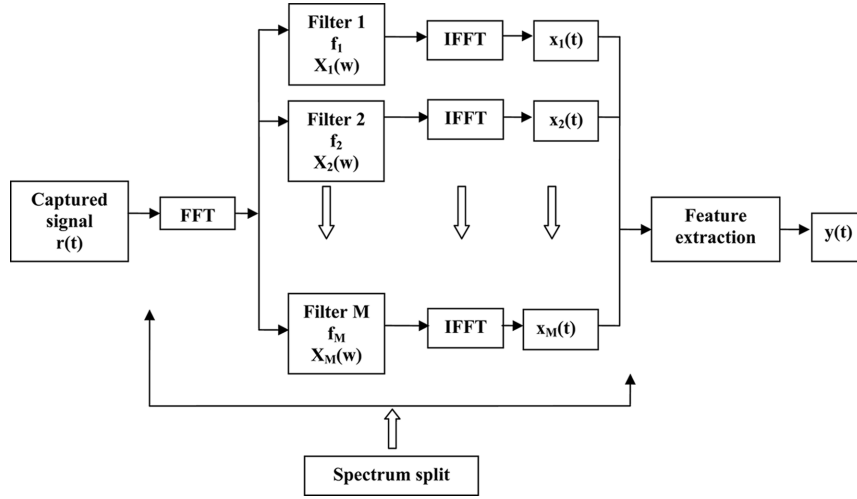


Fig. 2 Schematic flow chart of SSP

there is no damage or the incident and damage-scattered waves when there is damage), $s(t)$, activated at a certain central frequency and located in the main frequency band of the $r(t)$, and noise, $n(t)$, which can be described as

$$r(t) = s(t) + n(t), \quad 0 \leq t \leq T \quad (3)$$

SNR is a measure to quantify how much a signal has been contaminated by noise, defined as (Karpur *et al.* 1992)

$$SNR = 10 \times \log_{10} \left(\frac{\sum_{t=0}^{t=T} s(t)^2}{\sum_{t=0}^{t=T} n(t)^2} \right) \quad (4)$$

where T is the signal time duration of $r(t)$.

The SSP procedure consists of two steps: 1) spectrum split and 2) feature extraction, as illustrated in Fig. 2 and detailed as follow.

2.2.1 Spectrum split

Fast Fourier transform (FFT)

The frequency-energy spectrum of the captured wave signal, $r(t)$, can be acquired using fast Fourier transform (FFT). The main frequency band of $r(t)$ is defined as a bandwidth where the frequency-energy spectrum has an energy level above a certain threshold (commonly a half the peak energy, known as the “half attenuation” convention (Bosch *et al.* 2005)), as illustrated in Fig. 3.

Band-pass filters

The main frequency band of $r(t)$ is then split into a series of overlapping frequency sub-bands ($X_i(\omega)$, $i=1 \sim M$) by a series of Gaussian band-pass filters with different central frequencies (f_i , $i=1 \sim M$) (illustrated in Fig. 3). The reason for using Gaussian band-pass filters is their good behavior in both time and frequency domains (Ericsson *et al.* 1992). The total number of Gaussian band-pass filters (M) is defined by (Bosch *et al.* 2008)

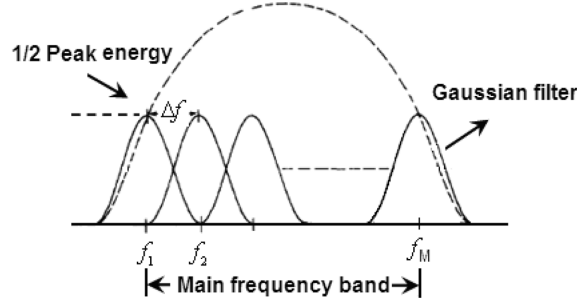


Fig. 3 Frequency spectrum distribution of a series of Gaussian band-pass filters

$$M = BT + 1 \tag{5}$$

where B is the main frequency bandwidth of $r(t)$, and T is the signal time duration of $r(t)$. The frequency interval (Δf) between the central frequencies of two neighboring Gaussian band-pass filters is defined by

$$\Delta f = 1/T \tag{6}$$

and the bandwidth of an individual Gaussian band-pass filter is defined as $2 \times \Delta f$ to minimize the possibility of signal frequency component leakage (Bosch *et al.* 2008).

Inverse fast Fourier transform (IFFT)

The M -split frequency sub-bands ($X_i(\omega)$, $i=1 \sim M$) are further processed using inverse fast Fourier transform (IFFT) to construct M corresponding time scale signals

$$x_i(t) = \frac{1}{2\pi} \int_{-\infty}^{\infty} X_i(\omega) \cdot e^{i\omega t} d\omega \tag{7}$$

In this study, the instantaneous amplitude variation range among the M constructed time scale signals ($x_i(t)$, $i=1 \sim M$) is defined as the instantaneous amplitude variation degree (IAVD) of $r(t)$

$$IAVD(t) = x_{max}(t) - x_{min}(t) \tag{8}$$

where $x_{max}(t)$ and $x_{min}(t)$ are the maximum and minimum of the magnitudes of ($x_i(t)$, $i=1 \sim M$) at the corresponding sampling time point respectively

$$x_{min}(t) = \min(x_1(t), x_2(t) \dots x_i(t) \dots x_M(t))$$

$$x_{max}(t) = \max(x_1(t), x_2(t) \dots x_i(t) \dots x_M(t))$$

When the target echo, $s(t)$, activated at a certain central frequency and located in the main frequency band of $r(t)$, appears, $x_i(t)$ ($i=1 \sim M$) all present M coherent instantaneous amplitudes, thereby producing a small instantaneous amplitude variation range with a small IAVD value. However, for other sections of $r(t)$, which are not in the main frequency band of $r(t)$, the M instantaneous amplitudes show great differences among each other, producing a large IAVD value. Moreover, SSP is a kind of non-linear filter method which acts on the split frequency sub-bands for the purpose of improving SNR and therefore the coherence degree of the M instantaneous amplitudes is only slightly influenced by noise

(Ericsson *et al.* 1992).

2.2.2 Feature extraction

A feature extraction algorithm is developed to determine the ToF of damaged-scattered waves by comparing the IAVD ($IAVD_{damage}(t)$) of the captured wave signal for the damage case ($r_{damage}(t)$) with that ($IAVD_{benchmark}(t)$) of the captured wave signal for the benchmark ($r_{benchmark}(t)$) before the damage exists. As a wave mode (the incident wave and damage-scattered wave) is normally at a certain activated central frequency and located in the main frequency band of the captured wave signals for both the damage case and the benchmark, when the incident wave appears in $r_{damage}(t)$ and $r_{benchmark}(t)$, the $IAVD_{damage}(t)$ and $IAVD_{benchmark}(t)$ are both small and their differences are also small (they are not identical because of the system difference between benchmark and damage case). However, when the damage-scattered wave appears in $r_{damage}(t)$ but not in $r_{benchmark}(t)$, the $IAVD_{damage}(t)$ is small whereas the $IAVD_{benchmark}(t)$ is large, and there are large differences between them. Therefore, it can be deduced that the moment with small values for the $IAVD_{damage}(t)$ but large values for the $IAVD_{benchmark}(t)$ correspond to the appearance of the damage-scattered S_0 mode. In this study, the difference between the and the $IAVD_{benchmark}(t)$, $\Delta(t)$, is calculated to determine the appearance of the damage-scattered S_0 mode. The $\Delta(t)$ when the incident S_0 mode propagating directly from the actuator to the sensor arrives (T_{A-S}) is set as a threshold, ΔT_{A-S} , to calibrate the system difference at two different status. T_{A-S} can be determined based on the propagation group velocity of the S_0 mode and the distance between the actuator and the sensor. Between T_{A-S} and the arrival moment of boundary reflection, the appearance of the damage-scattered S_0 mode can be deduced at the moment when $\Delta(t)$ is larger than ΔT_{A-S} . For the purpose of indicating the corresponding time, the output of the proposed SSP method, $y(t)$, is set as the magnitude of $r_{damage}(t)$ when $\Delta(t)$ exceeds ΔT_{A-S} , otherwise, it is set as zero. The feature extraction algorithm can be detailed as

$$\Delta(t) = IAVD_{benchmark}(t) - IAVD_{damage}(t), \quad 0 \leq t \leq T \quad (9)$$

$$y(t) = \begin{cases} r_{damage}(t), & \Delta(t) > \Delta T_{A-S} \\ 0, & else \end{cases} \quad (10)$$

The first sampling time point with $y(t)$ not equal to zero after T_{A-S} is defined as T_{A-D-S} . Substituting T_{A-S} and T_{A-D-S} into Eq. (1), the ToF of the damage-scattered S_0 mode (T_D) is determined and then the locus of the damage edge is configured.

3. Experimental set-up

An intact aluminum plate ($600 \times 600 \times 2.0$ mm), as the benchmark, was first assessed using Lamb wave signals in an ideal working environment. To ensure that the benchmark wave signals were indeed captured in an ideal laboratory condition, the intact aluminum plate was mounted on a vibration isolation table which provided a vibration-free working environment. Four circular piezoelectric transducers (PZT PI PIC151, PRYY-0929) with diameter of 6.9 mm and thickness of 0.5 mm (from P1 to P4) were surface-mounted on the plate, functioning as an active sensor network (Fig. 4). Each PZT wafer acted in turn as an actuator to activate Lamb waves while the others

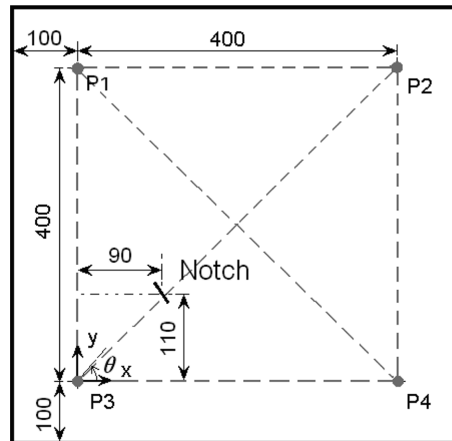


Fig. 4 Schematic diagram of a specimen with an active sensor network and the six selected sensing paths

functioned as sensors to capture wave signals propagating in the aluminum plate. A coordinate system with the origin set at P3 was used to locate the inspected area (400×400 mm) which was covered by six selected sensing paths (dashed lines in Fig. 4). A through-thickness notch of 30 mm length, 125° orientation to the x axis was introduced by a blade of 0.6 mm thickness at the coordinate of (90, 110). The notched aluminum plate (the damage case) was then assessed again, using Lamb wave signals. In practical application, noise (such as environment noise and electromagnetism disturbance from other systems) is usually blended into the captured Lamb wave signals. To model a working environment with indeterminate noise, synthetic broadband ‘white’ noise was added into the captured wave signal for the damage case in the experiment.

The wave signals were activated and captured using a system developed on the VXI platform consisting of an arbitrary signal generator (Agilent E1441), signal amplifier (PiezoSys EPA-104), signal conditioner (Agilent E3242A), and signal digitizer (Agilent E1437A). A 5-cycle sinusoidal tone burst (60 V peak-to-peak) pulsed by a Hanning window at a central frequency of 300 kHz was used for wave activation. The wave signals were captured at a sampling rate of 20.48 MHz and the sampling time duration for each signal was set as $200 \mu\text{s}$.

4. Results and discussion

The propagation group velocity of the S_0 mode (v_g) was defined as 5190 m/s in the intact aluminum plate, based on an average propagation time (T_{A-S}) of $77 \mu\text{s}$ for a propagation distance of 400 mm.

4.1 Damage identification using SSP

The wave signals captured from sensing path P3-P4 (when P3 was actuator and P4 was sensor) were exemplified during evaluation of the proposed SSP method and Hilbert transform. All captured wave signals were identically normalized.

4.1.1 Without noise

In the ideal working environment, only slight differences in magnitude and amplitude were observed between the captured wave signals for the benchmark and the damage case, as zoomed in Fig. 5. The frequency-energy spectra of the captured wave signals without noise were acquired using FFT, as shown in Fig. 6. The coupling condition between piezoelectric transducer and the aluminum plate and the frequency dispersion of Lamb waves caused that the central frequencies of the captured wave signals were not the activated 300 kHz exactly.

The main frequency bandwidth of the captured wave signal for the benchmark was

$$B = 70 \text{ kHz}$$

which was designated from 295 kHz to 365 kHz. The sampling time duration was

$$T = 200 \mu\text{s}$$

Based on Eqs. (5) and (6), the total number of band-pass filters was

$$M = 15$$

and the frequency interval between the central frequencies of two neighboring filters was

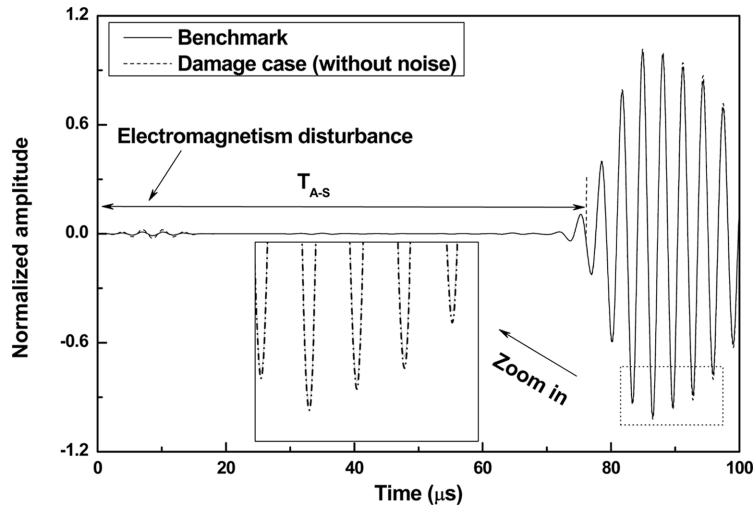


Fig. 5 Captured wave signals for the benchmark and the damage case without noise

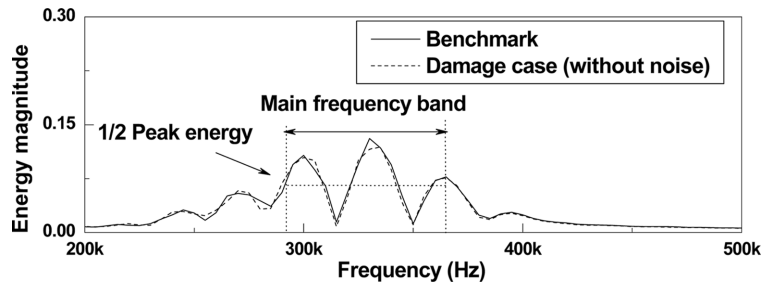


Fig. 6 Frequency-energy spectra of the captured wave signals for the benchmark and the damage case without noise

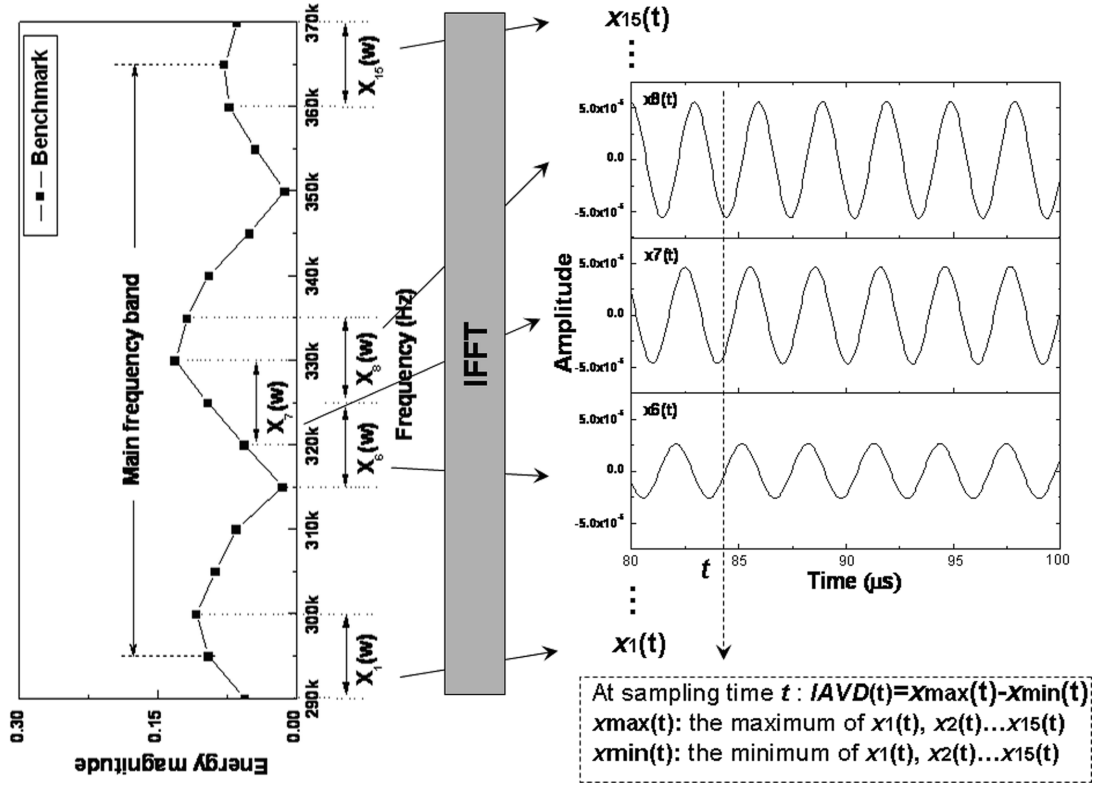


Fig. 7 Schematic flow chart of constructing time scale signals (exemplified by $x_6(t)$, $x_7(t)$ and $x_8(t)$) and calibrating $IAVD(t)$ of the captured wave signal for the benchmark

$$\Delta f = 5 \text{ kHz}$$

A series of Gaussian band-pass filters was designed and used to split the main frequency band into 15 overlapping frequency sub-bands ($X_i(\omega)$, $i=1\sim 15$), as illustrated in Fig. 7. Then, applying IFFT, 15 time scale signals ($x_i(t)$, $i=1\sim 15$) were constructed for the captured wave signal for the benchmark, with $x_6(t)$, $x_7(t)$, and $x_8(t)$ exemplified in Fig. 7.

For the captured wave signal for the damage case, the frequency band from 295 kHz to 365 kHz was also split by the series of Gaussian band-pass filters, and 15 time scale signals were constructed accordingly. Based on Eqs. (8) and (9), at each sampling point, the $IAVD_{benchmark}(t)$, and $\Delta(t)$ were acquired, as shown in Figs. 8(a) and (b). The threshold ($\Delta(T_{A-S})$) was defined at T_{A-S} ($77 \mu s$), as marked in Fig. 8(b). Based on Eq. (10), $y(t)$ was acquired (Fig. 8(c)), and T_{A-D-S} was determined

Table 1 Identification results using two methods

Identification method	Noise	Identified center [mm]	Relative distance [mm]
SSP	Without	(117, 128)	32.59
	With (SNR=1 dB)	(109, 136)	32.48
Hilbert transform	Without	(122, 101)	33.17
	With (SNR=1 dB)	Fail	Fail

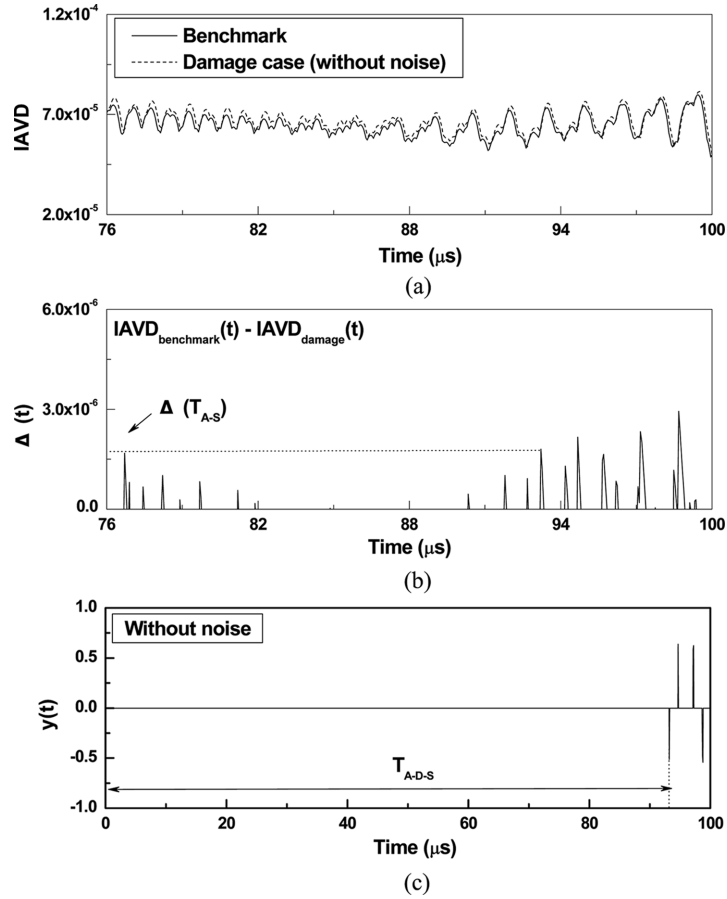


Fig. 8 (a) $IAVD_{benchmark}(t)$ and $IAVD_{damage}(t)$, (b) $\Delta(t)$ and (c) $y(t)$ without noises

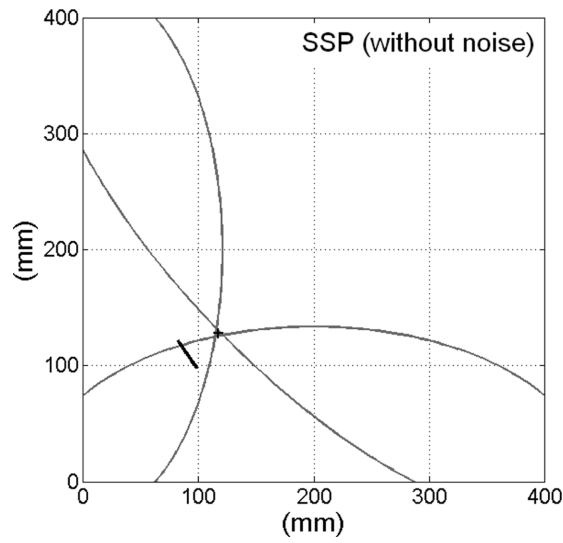


Fig. 9 Identification result using SSP method without noise

at 93 μs . Substituting T_{A-S} and T_{A-D-S} into Eq. (1), T_D was determined.

Then T_D was determined by the same way when P4 was actuator and P3 was sensor. The average of two determined T_D was used to configure the corresponding ellipse locus for sensing path P3-P4. With each determined T_D from individual sensing paths of the active sensor network, the damage was identified in the inspected area using the triangulation algorithm and its center (with the minimum distance summation to the individual loci) was marked as '+', as shown in Fig. 9. The coordinate of the identified center and its relative distance from the actual center were summarized in Table 1.

4.1.2 With noise

When a captured wave signal for a damage case was contaminated by broadband 'white' noise, the more seriously the signal was contaminated, the lower was the SNR. Four contaminated cases for captured wave signals with different SNRs of 13 dB, 8 dB, 5 dB and 1 dB were shown in Fig. 10. The captured wave signal with the lowest SNR (SNR=1 dB, the most contaminated) was processed using the SSP method, as an example. Its frequency-energy spectrum was shown in Fig. 11. In comparison with Fig. 6, it was evident that the noise energy distorted the energy distribution of the captured wave signal seriously. As described in Section 4.1.1, the IAVD of the captured wave signal for the damage case with SNR of 1 dB ($IAVD_{damage(SNR=1dB)}(t)$), $\Delta(t)$ and $y(t)$ were acquired (Fig. 12) and T_{A-D-S} was determined at 94 μs accordingly. The identification result using the SSP method

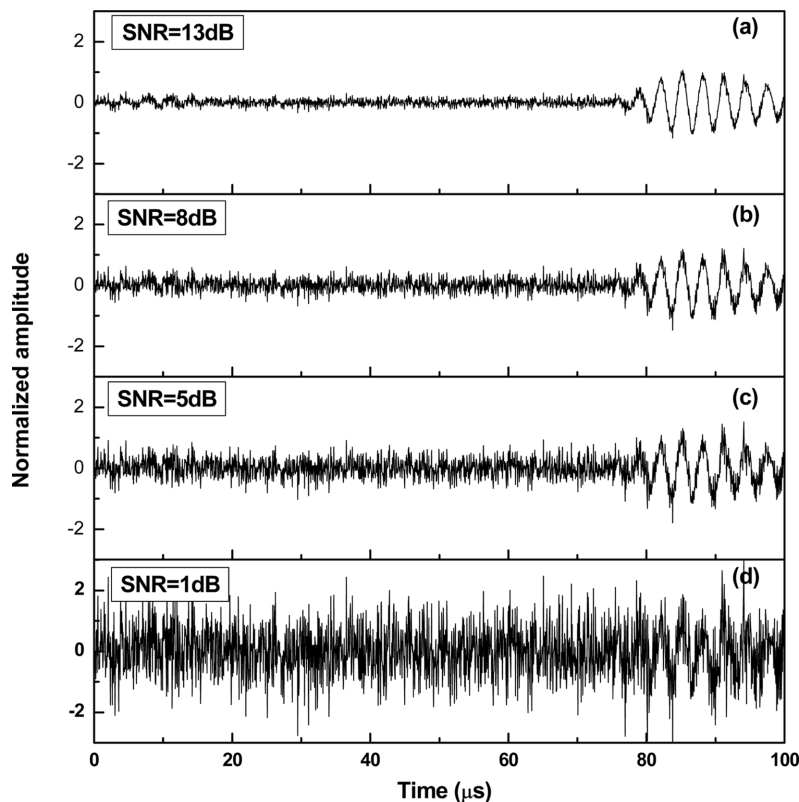


Fig. 10 Captured wave signal for the damage case with (a) SNR=13 dB, (b) SNR=8 dB, (c) SNR=5 dB and (d) SNR=1 dB

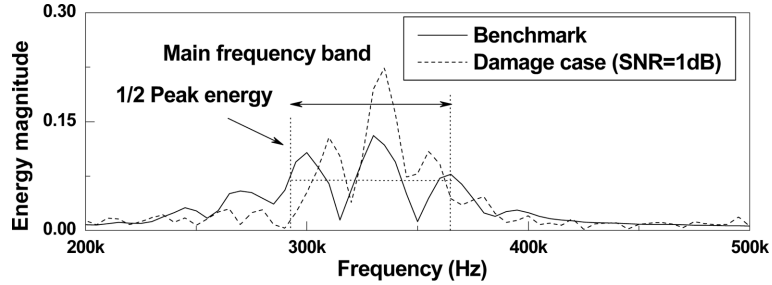


Fig. 11 Frequency-energy spectra of the captured wave signals for the benchmark and the damage case with noise (SNR=1 dB)

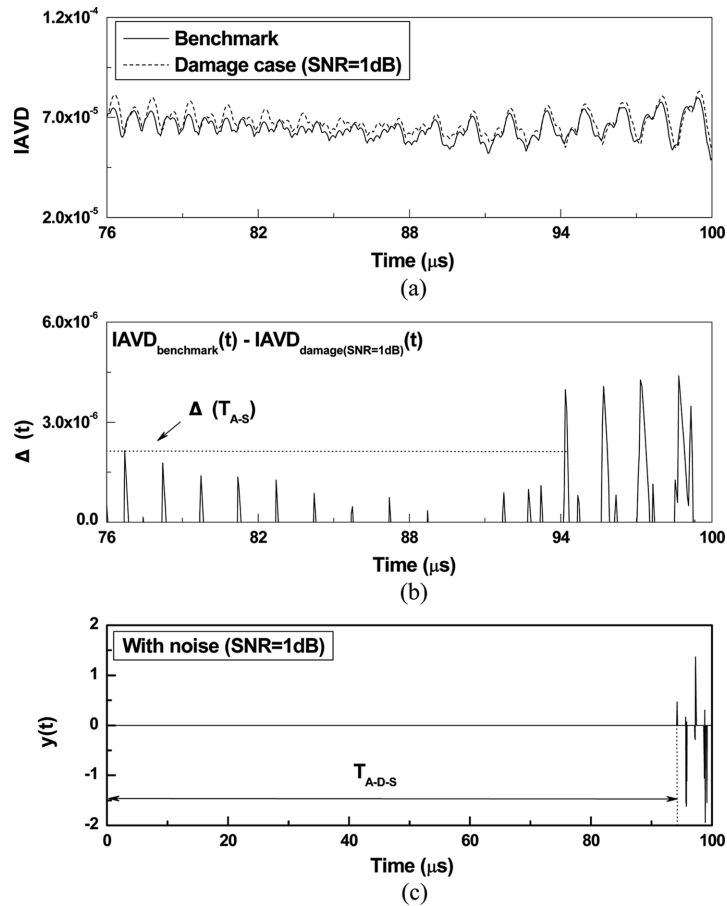


Fig. 12 (a) $IAVD_{benchmark}(t)$ and $IAVD_{damage(SNR=1dB)}(t)$, (b) $\Delta(t)$ and (c) $y(t)$ with noise (SNR=1 dB)

with noise (SNR=1 dB) was shown in Fig. 13 and summarized in Table 1. Using the SSP method the notch location was identified successfully with an acceptable error (32.59 mm off the actual location without noise; 32.48 mm with noise) based on the determined ToF of the damage-scattered S_0 mode, regardless of whether the captured wave signal was overwhelmed by the strong broadband ‘white’ noise, demonstrating that the proposed SSP method has great tolerance of broadband noise.

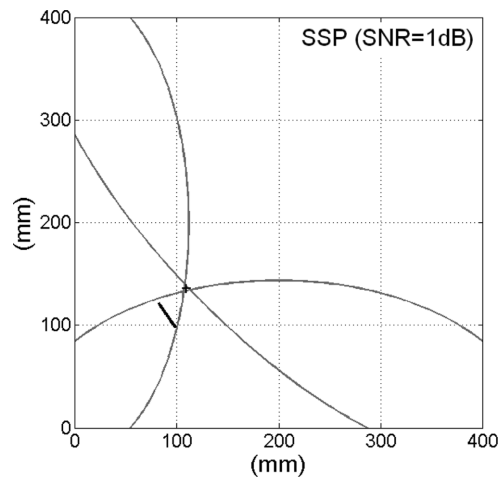


Fig. 13 Identification result using SSP method with noise (SNR=1 dB)

4.2 Damage identification using Hilbert transform

4.2.1 Without noise

When the wave signal for a damage case was captured in an ideal working environment, the benchmark wave signal could be subtracted from it to interpret a damage-scattered wave signal (Lu *et al.* 2010). The acquired damage-scattered wave signal was shown in Fig. 14(a). The wave

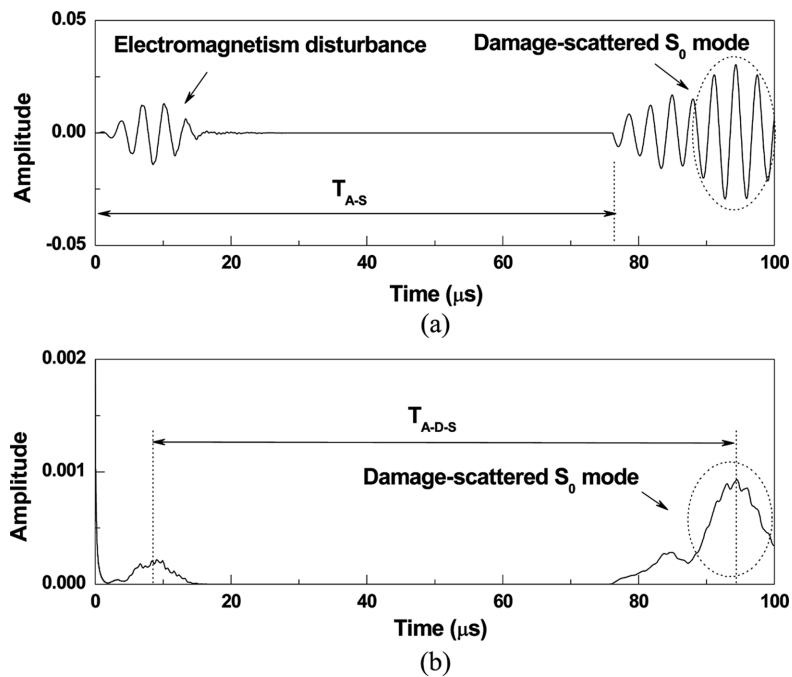


Fig. 14 (a) Damage-scattered wave signal without noise and (b) its energy distribution using Hilbert transform

package at the beginning was caused by electromagnetism disturbance when Lamb waves were activated. T_{A-S} was known at $77 \mu s$ and

$$T_{A-D-S} > T_{A-S}$$

Therefore the first wave package after T_{A-S} was identified as the damage-scattered S_0 mode. Based on the energy distribution of the damage-scattered wave signal acquired by using the Hilbert transform, as shown in Fig. 14(b), T_{A-D-S} was determined as the time lag from $8 \mu s$ to $95 \mu s$, i.e., the time lag between the peak energy of the activated wave signal and that of the damage-scattered S_0 mode. Eventually, the notch was identified in the ideal working environment, using the triangulation algorithm, with an error of 33.17 mm, as shown in Fig. 15 and summarized in Table 1.

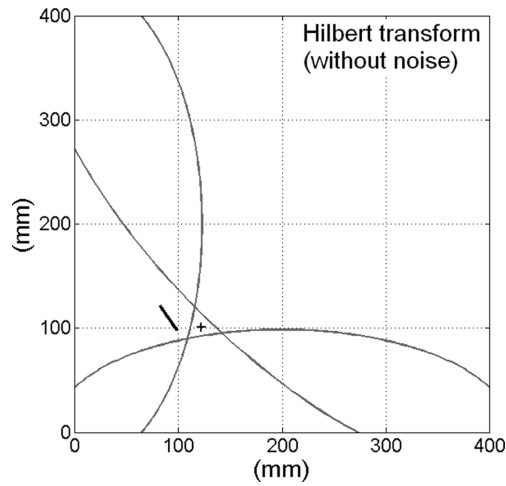


Fig. 15 Identification result using Hilbert transform without noise

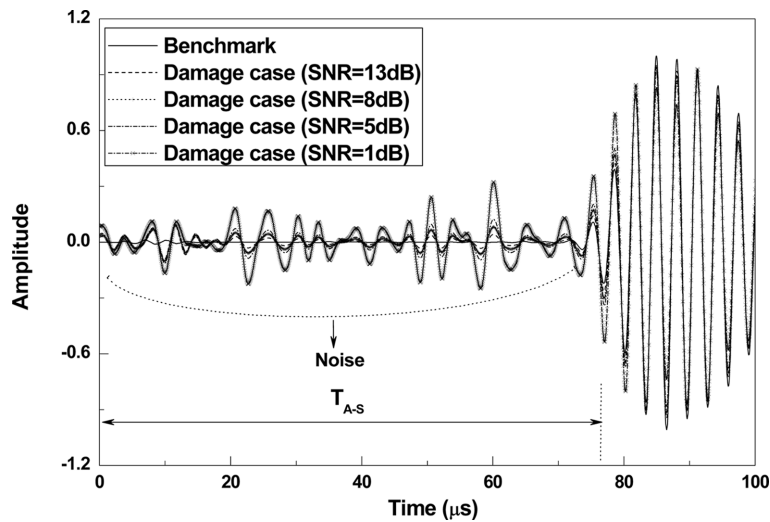


Fig. 16 Comparison of the captured wave signal for the benchmark and the de-noised signals shown in Figure 10 using DWT (db 10)

4.2.2 With noise

To exclude the noise disturbance as much as possible, the captured wave signals for the damage case with noise (Fig. 10) were processed using a discrete wavelet transform (DWT, db10), following well established procedure (Su *et al.* 2009), creating de-noised signals (Fig. 16). Even for the de-noised signal, compared to the benchmark, there was evident noise before the incident S_0 mode arrived, demonstrating that the noise could not be effectively filtered. Then the captured wave signal for the benchmark was subtracted from the de-noised signal to interpret the damage-scattered wave signal (Fig. 17(a)), and its energy distribution was acquired (Fig. 17(b)). As described in Section 4.2.1, the first wave package after T_{A-S} was identified as the damage-scattered S_0 mode. To allow comparison with the identification results in Section 4.1.2, take the captured wave signal with the

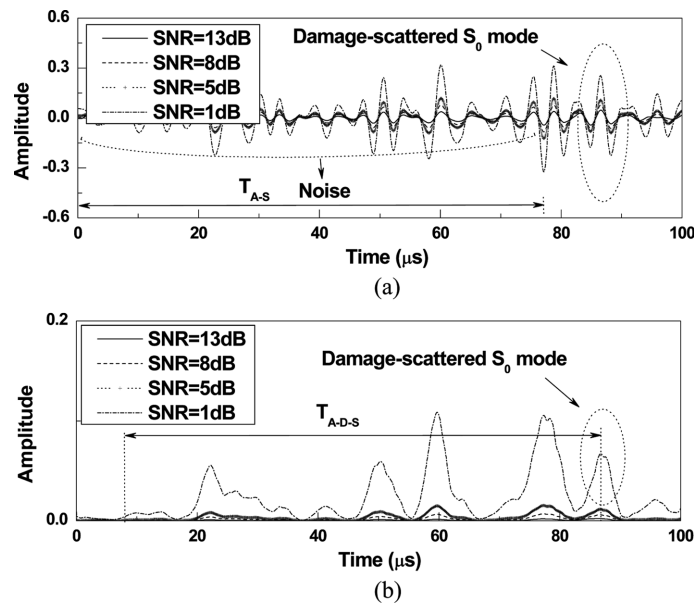


Fig. 17 Damage-scattered wave signal with noise and (b) its energy distribution using Hilbert transform

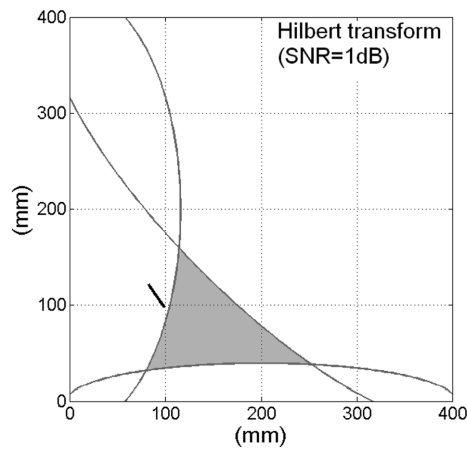


Fig. 18 Identification result using Hilbert transform with noise (SNR=1 dB)

SNR of 1 dB as an example, T_{A-D-S} was determined as the time lag from $8 \mu\text{s}$ to $87 \mu\text{s}$. As a result, the intersection of the multiple loci configured by the multiple sensing paths of the active sensor network was so large that it lost its focus for locating the damage, as shown in Fig. 18. It can be concluded that the ToF of the damage-scattered S_0 mode determined using the Hilbert transform is effective only in the ideal working environment, and its precision decreases when the captured wave signal is contaminated by broadband noise.

4.3 Discussion

Comparing the damage identification results using the proposed SSP method with those using the Hilbert transform in noisy environment, it was obvious that the SSP method was more robust to resist the disturbance of noise. The high sampling rate (20.48 MHz) was necessary to make sure of the precise captured wave signal in the time domain because of the high propagation velocity of Lamb waves. For such a sampling rate, the analyzed frequency bandwidth of the captured wave signal was fixed as 160 kHz (from 160 kHz to 320 kHz in the 6th decomposed level) using the DWT method. Noise could not be filtered efficiently in the relative broad frequency band. However, in SSP, the main frequency band of the captured wave signal was split into a series of narrow overlapping frequency sub-bands (with frequency bandwidth of 10 kHz) by a series of band-pass filters, and the developed feature extraction algorithm was applied on individual narrow frequency sub-band. Therefore the proposed SSP method was capable of filtering the noise with more efficiency and identifying the damage-scattered S_0 mode with higher precision.

5. Conclusions

A SSP method was developed to determine the ToF of damage-scattered wave in this study. The efficiency in determining the ToF of the damage-scattered S_0 mode was experimentally evaluated for the SSP method and the Hilbert transform in both ideal and noisy working environments. Using the Hilbert transform on the damage-scattered wave signal, the ToF of the damage-scattered S_0 mode was determined based on the energy distribution and the notch was identified in the ideal working environment. However, when the captured wave signal was contaminated by broadband noise which could not be filtered efficiently, the noise energy overwhelmed the energy of the damage-scattered waves, causing a large error in the ToF determination and leading to failure of damage identification in the noisy working environment. The proposed SSP method determined the ToF of damage-scattered S_0 mode by comparing the IAVD of the captured wave signals for the damage case with that for the benchmark. The IAVD of the captured wave signal calibrated using the SSP method was only slightly influenced by the noise energy, so that the ToF of the damage-scattered S_0 mode could be determined with high precision not only in the ideal working environment but also in a noisy working environment, even when the captured wave signal was severely overwhelmed by strong broadband ‘white’ noise. The identification results demonstrated that the proposed SSP method has a high capacity to resist noise disturbance during guided wave-based damage identification.

Acknowledgements

The authors are grateful for the research support received from the National Natural Science

Foundation of China (NSFC No. 10702041, 11072148 and 11061160491). X. Miao is grateful for the living support of the State Scholarship Fund from the China Scholarship Council. L. Ye and Y. Lu are grateful for the research support of a Discovery Project (DP) and an Australian Postdoctoral Fellowship (ARC-APD) from the Australian Research Council, respectively.

References

- Benammar, A., Drai, R. and Guessoum, A. (2008), "Detection of delamination defects in CFRP materials using ultrasonic signal processing", *Ultrasonics*, **48**(8), 731-738.
- Bosch, I. and Vergara, L. (2008), "Normalized split-spectrum: a detection approach", *Ultrasonics*, **48**(1), 56-65.
- Bosch, I. and Vergara, L. (2005), "New insights and extensions of split-spectrum algorithms from an optimum distributed detection perspective", *Proceedings of the IEEE Ultrasonics Symposium*, Polytechnic University of Valencia, September.
- Diamanti, K., Soutis, C. and Hodgkinson, J.M. (2005), "Lamb waves for the non-destructive inspection of monolithic and sandwich composite beams", *Compos. Part A - Appl S.*, **36**(2), 189-195.
- Ericsson, L. and Stepinski, T. (1992), "Cut spectrum processing: a novel signal processing algorithm for ultrasonic flaw detection", *NDT & E. Int.*, **25**(2), 59-64.
- Giurgiutiu, V. (2005), "Tuned lamb wave excitation and detection with piezoelectric wafer active sensors for structural health monitoring", *J. Intell. Mater. Syst. Struct.*, **16**(4), 291-305.
- Ip, K.H., Tse, P.W. and Tam, H.Y. (2004), "Extraction of patch-induced Lamb waves using a wavelet transform", *Smart Mater. Struct.*, **13**(4), 861-872.
- Karpur, P. and Canelones, O.J. (1992), "Split spectrum processing: A new filtering approach for improved signal-to-noise ratio enhancement of ultrasonic signals", *Ultrasonics*, **30**(6), 351-357.
- Kessler, S.S., Spearing, S.M. and Soutis, C. (2002), "Damage detection in composite materials using Lamb wave methods", *Smart Mater. Struct.*, **11**(2), 269-278.
- Li, F., Meng, G., Kageyama, K., Su, Z. and Ye, L. (2009), "Optimal mother Wavelet selection for lamb wave analyses", *J. Intell. Mater. Syst. Struct.*, **20**(10), 1147-1161.
- Lu, Y., Ye, L., Wang, D., Zhou, L. and Cheng, L. (2010), "Piezo-activated guided wave propagation and interaction with damage in tubular structures", *Smart. Struct. Syst.*, **6**(7), 835-849.
- Lu, Y., Ye, L., Wang, D., Wang, X. and Su, Z. (2010), "Conjunctive and compromised data fusion schemes for identification of multiple notches in an aluminium plate using lamb wave signals", *IEEE T. Ultrason. Ferr.*, **57**(9), 2005-2016.
- Michaels, J.E. (2008), "Detection, localization and characterization of damage in plates with an in situ array of spatially distributed ultrasonic sensors", *Smart Mater. Struct.*, **17**(3), 035035.
- Pardo, E., San Emeterio, J.L., Rodriguez, M.A. and Ramos, A. (2006), "Noise reduction in ultrasonic NDT using undecimated wavelet transforms", *Ultrasonics*, **44**(1), 1063-1067.
- Quek, S.T., Tua, P.S. and Wang, Q. (2003), "Detecting anomalies in beams and plate based on the Hilbert-Huang transform of real signals", *Smart Mater. Struct.*, **12**(3), 447-460.
- Su, Z., Yang, C., Pan, N., Ye, L. and Zhou, L.M. (2007), "Assessment of delamination in composite beams using shear horizontal (SH) wave mode", *Compos. Sci. Technol.*, **67**(2), 244-251.
- Su, Z. and Ye, L. (2009). *Identification of Damage Using Lamb Waves: From Fundamentals to Applications*, Springer-Verlag Berlin, Heidelberg.
- Su, Z., Ye, L. and Bu, X. (2002), "A damage identification technique for CF/EP composite laminates using distributed piezoelectric transducers", *Compos. Struct.*, **57**(1-4), 465-471.
- Wang, L. and Yuan, F.G. (2007), "Active damage localization technique based on energy propagation of Lamb waves", *Smart. Struct. Syst.*, **3**(2), 201-217.
- Wang, L. and Yuan, F.G. (2007), "Group velocity and characteristic wave curves of Lamb waves in composites: Modeling and experiments", *Compos. Sci. Technol.*, **67**(7-8), 1370-1384.